Preparation, Characterization, and Enzyme Immobilization Capacities of Superparamagnetic Silica/Iron Oxide Nanocomposites with Mesostructured Porosity

Teresa Valdés-Solís,[†] Aldo F. Rebolledo,[‡] Marta Sevilla,[†] Patricia Valle-Vigón, Oscar Bomatí-Miguel,[§] Antonio B. Fuertes,*[,†] and Pedro Tartaj*[,‡]

Instituto Nacional del Carbon (CSIC), Apartado 73, 33080 Oviedo, Spain, Instituto de Ciencia de Materiales de Madrid (CSIC), Cantoblanco 28049, Madrid, Spain, and Nanoporous Films and Particles Research Group, CiBER-BBN, Nanoscience Institute of Aragon, University of Zaragoza, C/Pedro Cerbuna 12, Zaragoza 50009, Spain

Received February 28, 2008. Revised Manuscript Received January 21, 2009

We present a method to produce superparamagnetic iron oxide/silica nanocomposites that have a large BET surface area, a high pore volume, and at least one pore size population centered at around or larger than 10 nm. By means of this methodology, which is based on nanocasting techniques, we are able to not only prepare mesoporous iron oxide/silica nanocomposites with adequate pore sizes and magnetic properties for enzyme immobilization but also explore various phenomena associated with the characteristics of the magnetic mesoporous matrixes. Magnetic nanocomposites that have a ordered mesostructured porosity, a high BET surface area, and a high pore volume display a better distribution of their magnetic components and superior magnetic properties than magnetic nanocomposites with a disordered mesostructured porosity and low BET surface area. The applicability of this kind of composites for the immobilization and magnetic separation of biomolecules has been clearly demonstrated in the case of lysozyme.

Introduction

The search for materials able to fulfill the requirements of biotechnological applications is behind many of the advances in the nanomaterials field. For example, biotechnological applications such as enzyme immobilization, drug delivery, or separation require nontoxic and stable superparamagnetic materials made up of a easily accessible and adjustable porous network that contains functional groups.[1] The most practical way to prepare these materials is to disperse, encapsulate, or coat iron oxide superparamagnetic nanoparticles in organic or inorganic matrixes. Thus, polymer organic matrixes that enhance stability and biocompatibility are frequently used to disperse magnetic nanoparticles.[1] Liposomes, polyelectrolyte multilayer microcapsules, or micelles are also typical examples of organic matrixes that can be used to encapsulate magnetic nanoparticles.[2] However, the use of organic matrixes can be problematic because of their limited chemical and mechanic stability, tendence to swell and susceptibility to microbiological contamination.[3] As an alternative, inorganic coatings do not experience swelling or porosity changes if the pH varies, and they are not vulnerable to microbial attack.[4] They also effectively protect doped molecules (enzymes, drugs, etc.) against the denaturation induced by extreme conditions of pH and temperature.[5] For applications such as the one we have in mind in this study (enzyme immobilization), inorganic matrixes are to be preferred. Of the inorganic matrixes available silica is the most suitable, as it ensures the presence of easily functionalizable surface silanol groups.[6] In addition, the silica surface confers a high stability on suspensions of particles at high volume fractions, when the pH changes or when the concentrations of electrolyte are high.[7]

In recent scientific literature, numerous examples can be found of the encapsulation of magnetic iron oxide nano-

* To whom correspondence must be addressed. E-mail: ptartaj@icmm.csic.es. E-mail: abefu@incar.csic.es.
[†] Instituto Nacional del Carbon (CSIC).
[‡] Instituto de Ciencia de Materiales de Madrid (CSIC).
[§] University of Zaragoza.

(1) (a) Pankhurst, Q. A.; Connolly, J.; Jones, S. K.; Dobson, J. *J. Phys. D: Appl. Phys.* **2003**, *36*, R167. (b) Tartaj, P. *Curr. Nanosci.* **2006**, *2*, 43. (c) Jeong, U.; Teng, X.; Wang, Y.; Xia, Y. N. *Adv. Mater.* **2007**, *19*, 33.
(2) (a) Caruso, F.; Trau, D.; Mohwald, H.; Renneberg, R. *Langmuir* **2000**, *16*, 1485. (b) Lavan, D. A.; Mcguire, T. *Nat. Biotechnol.* **2003**, *21*, 1184. (c) Sabate, R.; Barnadas-Rodriguez, R.; Callejas-Fernandez, J.; Hidalgo-Alvarez, R.; Estelrich, J. *Int. J. Pharm.* **2008**, *347*, 156.
(3) Arruebo, M.; Galan, M.; Navascues, N.; Téllez, C.; Marquina, C.; Ibarra, M. R.; Santamaría, J. *Chem. Mater.* **2006**, *18*, 1911.
(4) Weetal, H. H. *Biochim. Biophys. Acta* **1970**, *212*, 1.
(5) (a) Jain, T. K.; Roy, I.; De, T. K.; Maitra, A. N. *J. Am. Chem. Soc.* **1998**, *120*, 11092. (b) Roy, I.; Ohulchanskyy, T. Y.; Pudavar, H. E.; Bergey, E. J.; Oseroff, A. R.; Morgan, J.; Dougherty, T. J.; Prasad, P. N. *J. Am. Chem. Soc.* **2003**, *125*, 7860.
(6) (a) Ulman, A. *Chem. Rev.* **1996**, *96*, 1533. (b) Trewyn, B. G.; Slowing, I. I.; Giri, S.; Chen, H. T.; Lin, V. S. Y. *Acc. Chem. Res.* **2007**, *40*, 846.
(7) Mulvaney, P.; Liz-Marzán, L. M.; Giersig, M.; Ung, T. *J. Mater. Chem.* **2000**, *10*, 1259.
(8) (a) Philipse, A. P.; Vanbruggen, M. P. B.; Pathmamanoharan, C. *Langmuir* **1994**, *10*, 92. (b) Tartaj, P.; Gonzalez-Carreño, T.; Serna, C. *Adv. Mater.* **2001**, *13*, 1620. (c) Kim, B.-S.; Qiu, J.-M.; Wang, J.-P.; Taton, T. A. *Nano Lett.* **2005**, *10*, 1987. (d) Arruebo, M.; Fernandez-Pacheco, R.; Ibarra, R.; Santamaría, J. *Nano Today* **2007**, *2*, 22. (e) Kim, J.; Lee, J. E.; Lee, J.; Jang, Y.; Kim, S.-W.; An, K.; Yu, J. H.; Hyeon, T. *Angew. Chem., Int. Ed.* **2006**, *45*, 4789. (f) Salgueiriño-Maceira, V.; Correa-Duarte, M. A. *Adv. Mater.* **2007**, *19*, 4131.

10.1021/cm8005937 CCC: $40.75 © 2009 American Chemical Society
Published on Web 04/08/2009

particles.[1,8] There are also reports that deal with porous silica although in general these do not fully satisfy all the requirements for enzyme immobilization. Some methods produce materials that have a very low load of magnetic material and/or a pore size below 3−4 nm.[3,9] Substrates with pore sizes larger than 3−4 nm are essential for enzymes to be successfully immobilized as the latter are usually of a larger size. Some of the synthetic methods employed give rise to mesoporous magnetic composites with a high moment but such materials are not superparamagnetic (aggregation is favored) and again the pore size is around 3−4 nm.[10] Yet other methods lead to mesoporous composites with a homogeneous load of iron oxide of about 20 wt % but either the ordered mesoporous structure completely collapses at the temperature (1000 °C) at which the superparamagnetic phase develops[11] or the nanocomposites have a low surface area and the magnetic moment is very low.[12]

In the present work, we present a method to produce iron oxide/silica nanocomposites characterized by a high BET surface area, a large pore volume, a porosity made up of large mesopores (≥10 nm), and a superparamagnetic functionality provided by iron oxide nanosized $Fe^{III}_2Fe^{II}_{1-x}O_{4-x}$ spinel ferrites. Our aim was not only to prepare mesoporous iron oxide/silica nanocomposites with adequate pore sizes and magnetic properties for enzyme immobilization but also explore phenomena associated with the different characteristics of the resulting porous magnetic nanocomposites (mainly by correlating the textural characteristics with the magnetic and immobilization properties). Lysozyme was selected as a model enzyme for the immobilization studies. This is an antibacterial enzyme that is commercially very valuable. It has many uses in food processing and preservation as well as in the pharmaceutical industry.[13] Lysozyme (14.4 kDa) is a small globular protein with a prolate spheroid shape (4.5 × 3.0 × 3.0 nm) and it has been extensively used as a model for adsorption studies because of its wide availability, well-known structural characteristics, high stability against denaturation even after adsorption, and facile monitoring with UV/vis spectrophotometry.[14] For these reasons, this enzyme has often been used as a model for immobilization studies in silica[15] and carbon mesoporous materials.[16] Recently, our group used lysozyme to demonstrate the ability of carbon-based porous magnetic materials to immobilize biomolecules.[17]

Experimental Section

Preparation of the Silica Samples. Three types of mesoporous silica materials were selected as sacrificial templates: (a) an ordered mesostructured SBA-15 silica (denoted as S-SBA15), (b) a bimodal mesoporous silica with a spherical morphology (denoted as S-BIMODAL), and (c) a commercial mesoporous silica gel (Aldrich, Cat No. 28,851−9) (denoted as S-GEL). The ordered mesostructured SBA-15 silica with a plate-like morphology was synthesized according to the procedure reported in the literature.[18] Briefly, 1.3 g of surfactant Pluronic P123 was dissolved in a mixture of 10 g of water and 40 g of 2 M HCl, followed by the dropwise addition of 2.8 g of TEOS. The mixture was stirred for 5 min and then kept at 35 °C for 20 h, after which it was transferred to an autoclave and heated at 130 °C for 24 h. Finally, the sample was recovered by filtration, washed with abundant distilled water, dried, and calcined at 550 °C for 4 h. The spherical bimodal mesoporous silica was prepared as reported by Schulz-Ekloff et al.[19] In a typical synthesis, 2.5 g of CTAB (Cetyltrimethylammonium bromide, Aldrich) and 1.28 g of the silica source (Sodium Silicate, Aldrich) were dissolved in 45 g of water, followed by the addition of 3.95 g of ethyl acetate. The mixture was stirred for 30 s and then kept at room temperature for 5 h. It was then transferred to a closed Teflon vessel and kept at a temperature of 90 °C for 2 days. The solid product was filtered, washed with distilled water, dried, and calcined in air at 550 °C for 4 h.

Incorporation of Iron Oxide Spinel Nanoparticles within the Pores of the Silica. Nanosized $Fe^{III}_2Fe^{II}_{1-x}O_{4-x}$ spinels were incorporated following a methodology similar to that recently reported by our group.[20] First, the porosity of the silica was filled with a solution of iron nitrate in ethanol and then dried at 90 °C for 2 h. The amount of iron nitrate introduced was equivalent to around 20 and 32 wt % of the Fe_2O_3 present in the silica-iron oxide nanocomposite. Once the iron salt was deposited inside the pores of the silica, the sample was impregnated with ethylene glycol up to incipient wetness. The impregnated sample was then subjected to heat treatment under nitrogen up to a temperature of 450 °C (heating rate: 5 K/min) and kept at this temperature for 2 h. The different magnetic iron oxide/silica nanocomposites (FS) were labeled FyS-*x*, $y = 20$ or 32, indicating the percentage in Fe_2O_3 and x = SBA15, BIMODAL, or GEL referring to the type of the silica (S-SBA15, S-BIMODAL, or S-GEL) employed as template.

Enzyme Immobilization. Around 10 mg of the nanocomposite was dispersed at room temperature in 10 mL of lysozyme (Aldrich) solution (initial concentration of lysozyme: 1 mg mL^{-1}). The immobilization experiments were carried out in a closed vessel to avoid evaporation and at six different pH values: pH 6 (KH_2PO_4/

(9) (a) Köhn, R.; Paneva, D.; Dimitrov, M.; Tsoncheva, T.; Mitov, I.; Minchev, C.; Fröba, M. *Microporous Mesoporous Mater.* **2003**, *63*, 125. (b) Bourlinos, A. B.; Simopoulos, A.; Boukos, N.; Petridis, D. *J. Phys. Chem. B* **2001**, *105*, 2003. (c) Shokouhimehr, M.; Piao, Y. Z.; Kim, J.; Jang, Y. J.; Hyeon, T. *Angew. Chem., Int. Ed.* **2007**, *46*, 7039. (d) Deng, Y.; Qi, D.; Deng, C.; Zhang, X.; Zhao, D. *J. Am. Chem. Soc.* **2008**, *130*, 28.
(10) Zhao, W.; Gu, J.; Zhang, L.; Chen, H.; Shi, J. J. *J. Am. Chem. Soc.* **2005**, *127*, 8916.
(11) Nakamura, T.; Yamada, Y.; Yano, K. *J. Mater. Chem.* **2006**, *16*, 2417.
(12) Khalil, K. M. S.; Mahmoud, H. A.; Ali, T. T. *Langmuir* **2008**, *24*, 1037.
(13) Ghosh, R.; Cui, Z. F. *Biotechnol. Bioeng.* **2000**, *68*, 191.
(14) (a) Arai, T.; Norde, W. *Colloids Surf.* **1990**, *51*, 1. (b) Tortajada, M.; Ramon, D.; Beltran, D.; Amoros, P. *J. Mater. Chem.* **2005**, *15*, 3859. (c) Haynes, C. A.; Norde, W. *J. Colloid Interface Sci.* **1995**, *169*, 313. (d) Xiao, Q. G.; Tao, X.; Zou, H. K.; Chen, J. F. *Chem. Eng. J.* **2008**, *137*, 38.
(15) (a) Lei, J.; Yu, C.; Zhang, L.; Jiang, S.; Tu, B.; Zhao, D. *Microporous Mesoporous Mater.* **2004**, *73*, 121. (b) Vinu, A.; Murugesan, V.; Hartmann, M. *J. Phys. Chem. B* **2004**, *108*, 7323. (c) Wang, Y.; Caruso, F. *Chem. Mater.* **2005**, *17*, 953. (d) Kang, Y.; Shan, W.; Wu, J.; Zhang, Y.; Wang, X.; Yang, W.; Tang, Y. *Chem. Mater.* **2006**, *18*, 1861.
(16) (a) Vinu, A.; Miyahara, M.; Ariga, K. *J. Phys. Chem. B* **2005**, *109*, 6436. (b) Vinu, A.; Miyahara, M.; Sivamurugan, V.; Mori, T.; Ariga, K. *J. Mater. Chem.* **2005**, *15*, 5122. (c) Vinu, A.; Hossian, K. Z.; Srinivasu, P.; Miyahara, M.; Gokulakrishnan, N.; Mori, T.; Ariga, K.; Balasubramanian, V. V. *J. Mater. Chem.* **2007**, *17*, 5122.
(17) (a) Fuertes, A. B.; Sevilla, M.; Valdés-Solís, T.; Tartaj, P. *Chem. Mater.* **2007**, *19*, 5418. (b) Fuertes, A. B.; Sevilla, M.; Valdés-Solís, T.; Tartaj, P. *J. Phys. Chem. C* **2008**, *112*, 3648.
(18) Zhao, D.; Huo, Q.; Feng, J.; Chmelka, B. F.; Stucky, G. D. *J. Am. Chem. Soc.* **1998**, *120*, 6024.
(19) Schulz-Ekloff, G.; Rathousky, J.; Zukal, A. *Int. J. Inorg. Mater* **1999**, *1*, 97.
(20) (a) Fuertes, A. B.; Tartaj, P. *Chem. Mater.* **2006**, *18*, 1675. (b) Fuertes, A. B.; Tartaj, P. *Small* **2007**, *3*, 275. (c) Fuertes, A. B.; Sevilla, M.; Alvarez, S.; Valdés-Solís, T.; Tartaj, P. *Adv. Funct. Mater.* **2007**, *17*, 2321.

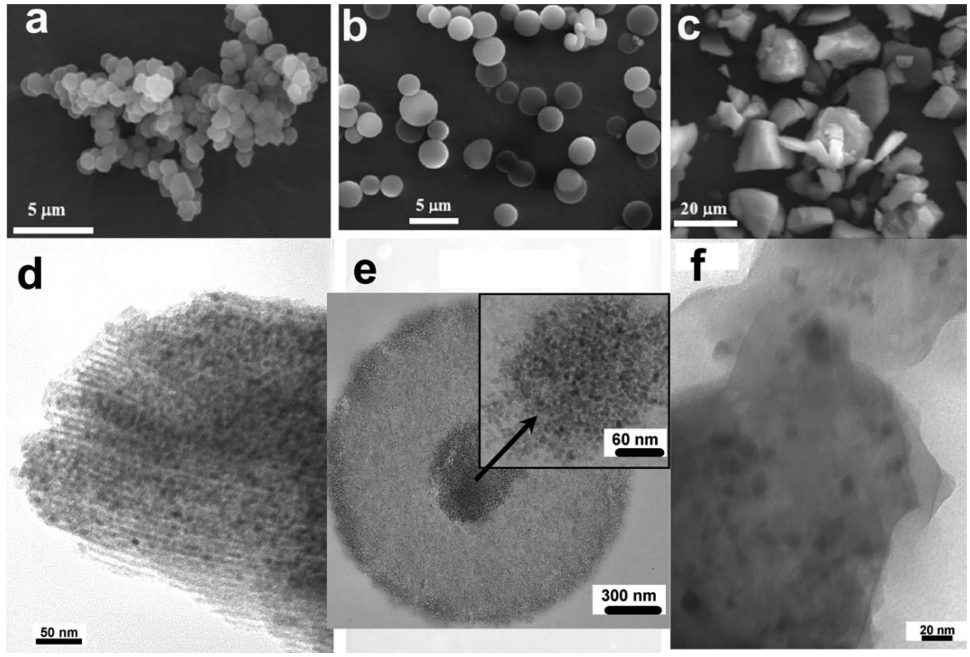

Figure 1. Typical SEM (upper) and TEM (lower) images obtained for the magnetic nanocomposites ((a, d) FS-SBA15; (b, e) FS-BIMODAL; (c, f) FS-GEL). The TEM image of the FS-BIMODAL is from a 90 nm ultramicrotomed sample to obtain better resolution. In this sample, low- and a high-magnification TEM pictures are displayed to show the presence of aggregates of magnetic nanoparticles, and that these aggregates are formed by nanoparticles of around the size estimated by XRD (6−7 nm). In the TEM images, the dark areas show the iron oxide spinel nanoparticles inserted inside the pores of the silica templates. The TEM images correspond to loadings of nanomagnets of 20 wt %.

NaOH buffer solution), pH 7 (KH_2PO_4/Na_2HPO_4 buffer solution), pH 9.2 (borax/NaOH buffer solution), pH 10 (borax/NaOH buffer solution), pH 10.5 ($NaHCO_3$/NaOH buffer solution), and pH 11 (Na_2HPO_4/NaOH buffer solution). All the buffer solutions were prepared in our laboratory with their ionic strength adjusted to ∼0.1 M. To evaluate the amount of enzyme immobilized, we periodically monitored the concentration of lysozyme in the solution by means of a UV−vis spectrophotometer (Shimadzu UV-2401PC) using UV absorption at 280 nm. Each experiment was continued until equilibrium was reached (typically a maximum of 120 h).

Characterization. X-ray diffraction (XRD) patterns were obtained on a Siemens D5000 instrument operating at 40 kV and 20 mA, using Cu Kα radiation. The morphology of the powders was examined by scanning (SEM, Zeiss DSM 942) and transmission (TEM, JEOL-2000 FXII) electron microscopy. Nitrogen adsorption and desorption isotherms were performed at −196 °C in a Micromeritics ASAP 2010 volumetric adsorption system. The BET surface area was deduced from the analysis of the isotherm in the relative pressure range of 0.04 to 0.20. The total pore volume was calculated from the amount adsorbed at a relative pressure of 0.99. The pore size distribution (PSD) was calculated by means of the Kruk−Jaroniec−Sayari method.[21] The saturation magnetization (M_s) and coercivity field values (H_c) were obtained from the magnetization curves recorded up to a field of 5T. For temperatures at which the magnetization curves appear unblocked, the M_s values were obtained from 1/H extrapolation at high fields (Langevin approach). For low temperatures (blocked regimes), the M_s values were obtained from the law of approach to saturation. Zero-field-cooling (ZFC) experiments were carried out to follow the dependence of magnetization on temperature. The ZFC curve was obtained by first cooling the system in a zero magnetic field down to 5 K. Then a magnetic field was applied (200 G), and the magnetization was measured as the temperature was increased. Decay of remanence data were obtained from the variation with temperature of the quotient M_r/M_s (where M_r is the remanence at zero field). The M_r/M_s values were obtained from the magnetization curves recorded below the blocking temperature. Fourier transform infrared spectra for lysozyme and lysozyme loaded on magnetic composite were recorded on a Nicolet 8700 spectrometer fitted with a diffuse reflection attachment.

(21) Kruk, M.; Jaroniec, M.; Sayari, M. *Langmuir* **1997**, *13*, 6267.

Results and Discussion

Structural Characteristics of the Magnetic Nanoparticle/Silica Nanocomposites. The morphology of the magnetic nanocomposites is illustrated in the SEM images shown in Figure 1. The (S-SBA15)-based magnetic nanocomposites that were obtained from highly ordered mesostructured SBA-15 silica particles consist of platelet-like particles with a diameter of ∼1−2 μm (see Figure 1a). The (S-BIMODAL)-based magnetic nanocomposites that were made from bimodal mesoporous silica exhibit a spherical morphology and have a particle diameter in the 2−4 μm range (see Figure 1b). The (S-GEL)-based magnetic nanocomposites obtained from a commercial mesoporous silica gel have an irregular shape (size ∼5−10 μm) (see Figure 1c). The formation of iron oxide nanosized $Fe^{III}_2Fe^{II}_{1-x}O_{4-x}$ spinel ferrites within the pores of silica was verified by X-ray diffraction (XRD). Thus, the XRD patterns shown in Figure 2 contain diffraction peaks characteristic of iron oxide spinel. The size of the crystallites estimated by applying the Scherrer equation to the (311) peak of the XRD patterns varies between 6 and 7 nm depending on the type of silica and the amount of iron oxide (see Table 1).

The iron oxide spinel nanoparticles are deposited inside the pores of the silica, as is clearly illustrated by the TEM images (Figure 1d−f). These images show that the nanoparticles (dark points) are distributed throughout the silica matrix. In the (S-SBA15)-based magnetic nanocomposites,

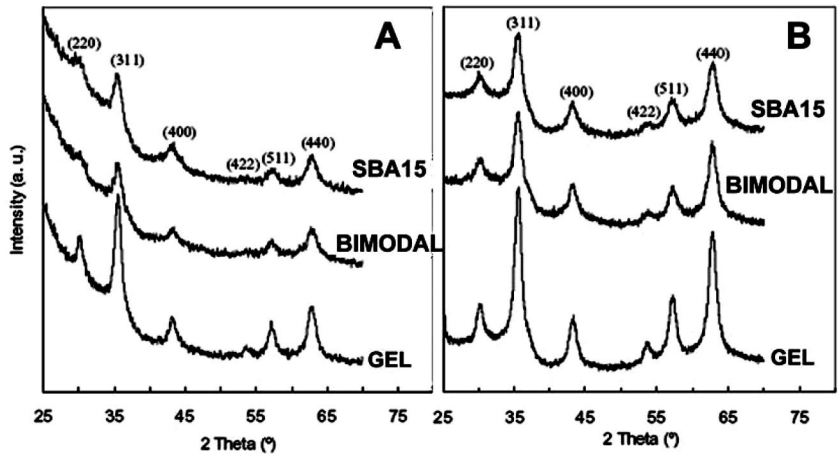

Figure 2. XRD patterns obtained for magnetic nanocomposites with a loading of nanomagnets of (A) 20 wt % and (B) 32 wt %. All the diffraction peaks are associated with the presence of iron oxide nanosized spinels (maghemite or magnetite).

Table 1. Physical Properties of the Silica Templates and Magnetic Nanocomposites; Saturation Magnetization (M_S) at Room Temperature, Temperature at Which ZFC Reaches Its Maximum (T_{max}), and Mean Blocking Temperature Derived from a Decay of the Remanence Fitting (T_B)

sample	Fe_2O_3(wt %)	S_{BET}(m^2 g^{-1})	V_p(cm^3 g^{-1})[a]	pore size (nm)[b]	d_{XRD} (nm)	M_S (emu g^{-1})[c]	T_{max} (K)	T_B (K)
S-SBA15		690	1.21	9.6				
F20S-SBA15	20	430	0.78 (0.15)	9.3	5.6	5.3 (27)	50	35
F32S-SBA15	32	330	0.56 (0.20)	8.9	6.2	12.1 (38)	55	37
S-BIMODAL		860	2.06	2.8, 27				
F20S-BIMODAL	20	520	1.30 (0.30)	2.5, 27	5.3	3.4 (17)	90	40
F32S-BIMODAL	32	340	0.76 (0.58)	26	6.5	9.3 (29)	100	46
S-GEL		340	0.84	12				
F20S-GEL	20	250	0.56 (0.07)	12	7	7.4 (37)	105	34
F32S-GEL	32	200	0.38 (0.13)	6, 12	7.2	15.6 (49)	110	36

[a] The values for the closed pore volumes (V^*-V_p) are presented in parentheses. [b] Maximum of pore size distributions. [c] The values for M_s normalized to iron oxide content are presented in parentheses.

the nanosized iron oxide ferrites are well-dispersed throughout the highly ordered pore structure characteristic of this type of matrix (Figure 1d). Aggregates of magnetic nanoparticles can be observed in the nanocomposites, which are made up of nanosized ferrites inserted inside the bimodal porosity of the spherical silica particles (see Figure 1e). Finally, for the nanocomposites obtained from silica gel, the ferrite nanoparticles have a distribution that ranges from highly dispersed to small clusters (see Figure 1f). Lattice fringes (and the corresponding electron diffractions obtained from the Fourier analysis) obtained from high-resolution TEM images confirm the presence of iron oxide nanosized $Fe^{III}_2Fe^{II}_{1-x}O_{4-x}$ spinel (Figure 3).

The textural characteristics of these magnetic nanocomposites as well as those of the silica samples are listed in Table 1. Both types of materials exhibit a high BET surface area, a large pore volume and a porosity made up almost exclusively of mesopores, as illustrated by the nitrogen sorption isotherms and the pore size distributions shown in Figure 4. These materials hardly contain any micropores, as can be deduced by applying the α_s-plot method to the adsorption branch of the N_2 isotherms. The incorporated magnetic nanoparticles cause a reduction in the textural properties of the nanocomposites with respect to those of the silica templates. This is evident from a comparison of the pore volumes of the silica templates and the magnetic nanocomposites (Table 1). Taking into account the volume occupied by the nanosized $Fe^{III}_2Fe^{II}_{1-x}O_{4-x}$ spinels (0.2 cm^3 g^{-1}, assuming a density of 5 g cm^{-3}) and the pore volume obtained for the silica samples, it is possible to calculate the unoccupied pore

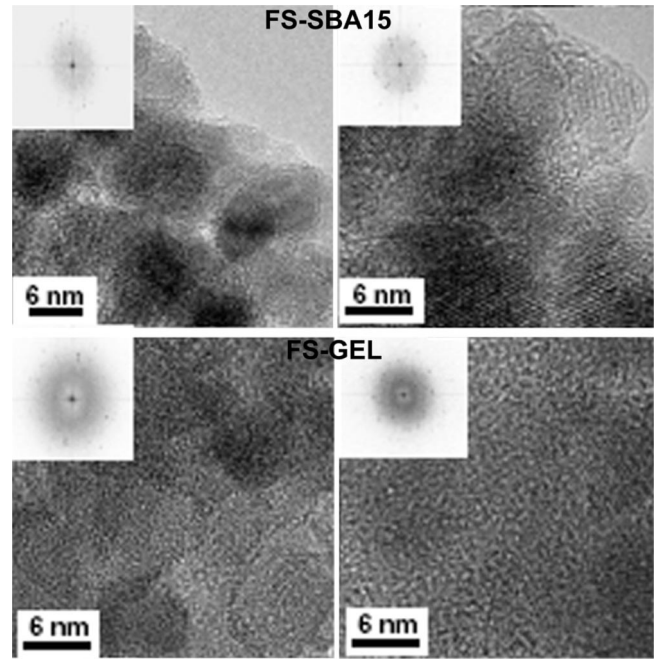

Figure 3. HR-TEM images of the magnetic nanocomposites (upper for FS-SBA15 and lower for FS-GEL) showing lattice fringes associated with differently oriented iron oxide nanosized $Fe^{III}_2Fe^{II}_{1-x}O_{4-x}$ spinels. The presence of aggregates in the FS-BIMODAL spherelike nanocomposites prevented us from obtaining images of nanosized ferrites with sufficient resolution.

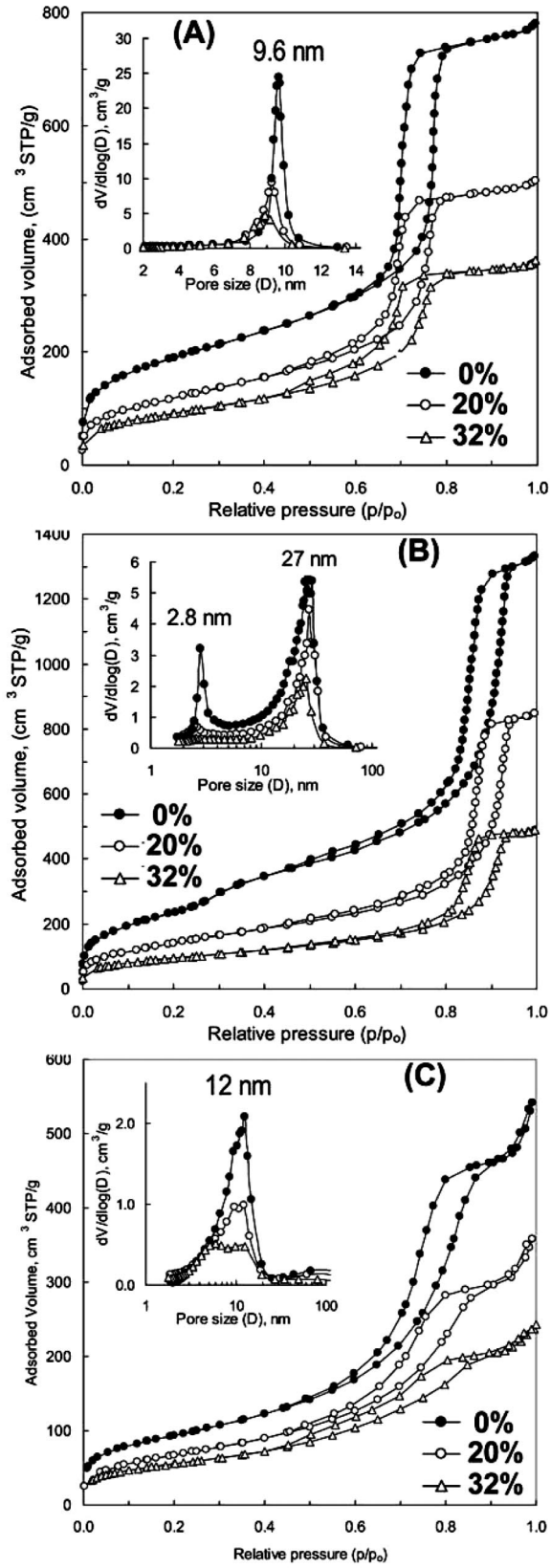

Figure 4. Nitrogen sorption isotherm and (inset) pore size distributions of the silica and magnetic nanocomposites. (A) S-SBA15, F20S-SBA15, F32S-SBA15; (B) S-BIMODAL, F20S-BIMODAL, F32S-BIMODAL; (C) S-GEL; F20S-GEL, F32S-GEL.

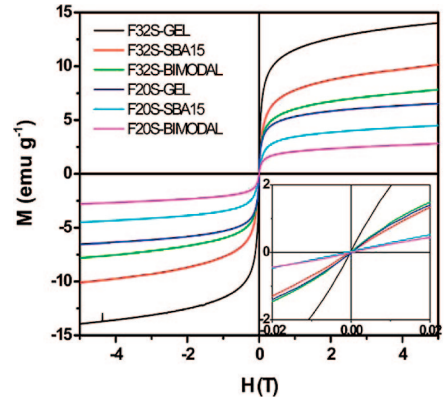

Figure 5. Magnetization curves (not normalized to the iron oxide content) of the magnetic nanocomposites at room temperature. Inset low field zoom showing zero coercivity.

volume for the composites (V^*). We observed that for all the composites the values obtained for V^* are greater than the experimentally measured ones (V_p). In our opinion the difference between both sets of values ($V^* - V_p$) is the closed pore volume generated by the nanosized iron oxide ferrites, as they possibly block the entrances to a number of pores. These values are listed in Table 1. It should also be pointed out that the composites obtained from the bimodal silica exhibit the largest closed pore volumes, 0.30 $cm^3\ g^{-1}$ (19% V^* for F20S-BIMODAL) and 0.58 $cm^3\ g^{-1}$ (43% V^* for F32S-BIMODAL). The bimodal silica contains two well-defined pore systems with sizes centered at 2.8 and 27 nm (see inset in Figure 4b). However, as the nanoparticles are deposited within the pores of the silica, the pore size distributions of the composites display a notable reduction in the number of pores of around 2.8 nm. Indeed, in the case of the F20S-BIMODAL composite this pore population has been drastically reduced, whereas for the F32S-BIMODAL composite has disappeared entirely. This suggests that the porosity has been completely obstructed by the deposited nanoparticles. What is more, a comparison of the V^* and V_p values for the composites obtained from the S-SBA15 and S-GEL templates also indicates closed pore volumes but to a lesser extent (Table 1). These results suggest that, like the (S-BIMODAL)-based composites, a fraction of the porosity has been completely obstructed by the deposited ferrite nanoparticles. It is also reasonable to assume that access to the nonblocked pores in these composites is partially restricted by the nanoparticles. In consequence, an increase in diffusional resistance can be expected in the pore networks of the composites compared to the silica templates. This hypothesis, as we will see below, has been confirmed by a notable reduction in the immobilization rate in the experiments performed to immobilize lysozyme in the silica samples and composites. Finally, we should point out that although the deposited nanoparticles lead to a certain obstruction of the porosity, these composites still retain a large BET surface area and a high pore volume, which means that a high fraction of the porosity is still accessible. This is important because it suggests that a significant fraction of the porosity in the silica matrix is available for immobilizing enzymes such as lysozyme.

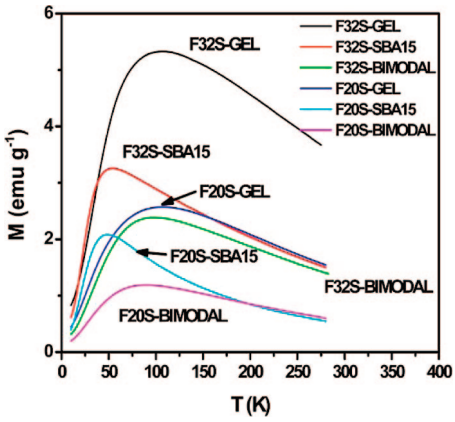

Figure 6. Zero-field-cooling (ZFCs) curves of the magnetic nanocomposites.

Magnetic Characterization of the Magnetic/Silica Nanocomposites. The magnetization reversal process was recorded at room temperature (RT) in order to check for superparamagnetic behavior in the samples (Figure 5). The samples have no magnetic memory (zero coercivity field). These results indicate that thermal energy plays a crucial role in the magnetism of the nanocomposites, as is usually the case in nanosized iron oxide ferrites of <10 nm.[1,20,22] In accordance with the presence of nanosized iron oxide ferrites, the saturation magnetization values (M_S) normalized to the iron oxide content were in all cases (from 15 to 50 emu g^{-1}) lower than those of the bulk (75−85 emu g^{-1}). The magnetic nanocomposites derived from the bimodal silica templates show values that are significantly lower (around 20−30% lower) than those determined for the (S-SBA15)-based samples, although they have a similar average crystallite size. The (S-GEL)-based composites contain spinels of a larger crystallite size and as a result a higher M_S can be expected, as was experimentally confirmed (Table 1).

Zero-field-cooling (ZFC) curves were recorded to obtain qualitative information on the blocking temperature (T_B) of the samples and the possible presence of interparticle interactions (Figure 6). In accordance with the absence of remanence at RT, the maximum of the ZFC curves peaks at a temperature (T_{max}) below RT (Figure 6, Table 1). In the framework of a Néel model, which assumes an assembly of independent single-domain particles, the ZFC might be expected to exhibit a maximum at the blocking temperature, T_B, at which point the relaxation time equals the time scale of the magnetization measurements. A distribution in particle size will result in a shift of the maximum to a temperature, $T_{max} = \beta\langle T_B\rangle$, where $\langle T_B\rangle$ is the mean blocking temperature and β is on the order of 1.0−2.0.[23] Dipolar interactions between the nanosized ferrites incorporated into the porous matrix also affect the temperature at which T_{max} appears (normally a shift to higher temperatures is observed) and make it difficult to estimate the real values of $\langle T_B\rangle$ from the ZFC curves.[23] However, in systems containing $Fe^{III}_2Fe^{II}_{1-x}O_{4-x}$ nanosized spinels, values of $\langle T_B\rangle$ can be derived from the decay of remanence as a function of temperature in the region where the nanocomposites are magnetically blocked, assuming a log-normal size distribution.[23] The $\langle T_B\rangle$ values obtained from this approach are also given in Table 1. Thus, from a comparison of the values of $\langle T_B\rangle$ derived from the ZFC curves and the values derived from the decay in remanence data for a particular sample, it is possible to draw conclusions about the blocking temperatures and the possible presence of dipolar interactions in the nanocomposites. Basically, we estimate an apparent value of $\langle T_B\rangle$ from the ZFC curve and we then compare this value with the real value derived from the remanence data. Dipolar interactions between the nanosized iron oxide ferrites cause the apparent value of $\langle T_B\rangle$ derived from the ZFC to be higher than the value derived from the remanence data. In the absence of interactions, the values of $\langle T_B\rangle$ estimated from ZFC and remanence data should be similar.

Table 1 summarizes the T_{max} results obtained from the ZFC curves ($\langle T_B\rangle = T_{max}/\beta$, where β can take values between 1 and 2) and the values of $\langle T_B\rangle$ derived from the remanence data. No significant dipolar interactions occur in the (S-SBA15)-based nanocomposites. The $\langle T_B\rangle$ values derived from the remanence data (35 K for F20S-SBA15 and 37 K for F32S-SBA15) are within the interval estimated from the ZFC curves (between 25 and 50 K for F20S-SBA15 and between 27 and 55 K for F32S-SBA15). However, a similar analysis of the ZFC and the remanence data shows the presence of significant dipolar interactions in the (S-BIMODAL) and (S-GEL)-based magnetic nanocomposites. For the bimodal samples the $\langle T_B\rangle$ values derived from the remanence data are lower (40 K for F20S-BIMODAL and 46 K for F32S-BIMODAL) than the interval estimated from the ZFC curves (between 45 and 90 K for F20S-BIMODAL and between 50 and 100 K for F32S-BIMODAL). The same result was obtained for the gel samples (34 and 36 K vs 52−105 and 55−110 K for F20S-GEL and F32S-GEL). These results are in accordance with the distribution observed by TEM and the magnetic moment values and crystallite sizes estimated from the magnetization curves and XRD. Dipolar interactions increase with μ^2r^6/D^3 (where μ is the magnetic moment, r is the iron oxide nanocrystallite radius, and D is the distance between the iron oxide nanocrystals). Thus, the (S-SBA15)-based nanocomposites, in which the magnetic nanoparticles are well-dispersed throughout the highly ordered pore structure (F20S-SBA15, F32S-SBA15, Figures 1 and 3), have intermediate magnetic moments and the smaller $Fe^{III}_2Fe^{II}_{1-x}O_{4-x}$ nanocrystals do not show significant interactions. In the (S-BIMODAL)-based samples, the aggregation observed by TEM (Figure 1) indicates that the interparticle distance between the nanomagnets is small, leading to an increase in dipolar interactions, despite the fact that these nanomagnets have the lowest magnetic moment and nanocrystal sizes (Table 1).[23] Finally, in the (S-GEL)-based nanocomposites, TEM observations revealed that the iron oxide nanoparticles are dispersed and form small clusters

(22) Roca, A. G.; Marco, J. F.; Morales, M. P.; Serna, C. J. *J. Phys. Chem. C* **2007**, *111*, 18577.
(23) (a) Gittleman, J. L.; Abeles, B.; Bozowsky, S. *Phys. Rev. B* **1974**, *9*, 3891. (b) Tartaj, P.; Gonzalez-Carreño, T.; Serna, C. *J. Phys. Chem. B* **2003**, *107*, 20. (c) Tartaj, P. *ChemPhysChem* **2003**, *4*, 1371. (d) Rebolledo, A. F.; Fuertes, A. B.; Gonzalez-Carreño, T.; Sevilla, M.; Valdés-Solís, T.; Tartaj, P. *Small* **2008**, *4*, 254.

(Figures 1 and 3). However, these samples exhibit the highest magnetic moments and crystallite sizes (Table 1). Strong dipolar interactions can therefore be predicted for these nanocomposites.

Immobilization of Lysozyme. To demonstrate the potential of the magnetic silica nanocomposites for immobilizing enzymes, we examined their ability to immobilize lysozyme. As was mentioned in the introduction section, lysozyme has been extensively used as a model enzyme for immobilization studies in silica and carbon mesoporous materials,[15−16] and has recently been selected by our group to demonstrate the ability of carbon-based porous magnetic materials to immobilize enzymes.[17]

The immobilization experiments were carried out over a wide range of pH values, i.e., between pH 6 and pH 11. At higher pH values (i.e., pH 12), the silica framework dissolves. Variation in the amounts of lysozyme adsorbed as a function of the pH of the solution is shown in Figure 7. We observed that for the silica samples (Figure 7a) and for the magnetic composites (panels b and c in Figure 7), the lysozyme uptake increases from pH 6 to pH 10−10.5, but decreases for higher pH values. The silica samples and the magnetic composites with 20 wt % ferrite also exhibit a clear maximum for enzyme immobilization at pH 10, whereas for the composite with 32 wt % ferrite, the maximum is at pH 10−10.5. What is especially remarkable is the large amount of lysozyme immobilized by the silica samples at pH 10 (840 mg g^{-1}, 860 mg g^{-1} and 560 mg g^{-1} for the S-BA15, S-BIMODAL, and S-GEL, respectively). These values are larger than those reported in the literature for similar substrates. For example, Vinu et al. obtained a lysozyme uptake of around 700 mg g^{-1} for a SBA-15 type silica (pH 9.6).[15b] The differences in the amount of lysozyme immobilized are probably related to the pH of the solution employed in each case. In fact, as is shown in Figure 7, small differences in the pH of solution may cause a large variation in immobilization uptakes. The incorporation of iron oxide nanoparticles leads to a decrease in the amount of lysozyme adsorbed in relation to the silica samples. Furthermore, the increase in iron oxide from 20 wt % (Figure 7b) to 32 wt % (Figure 7c) gives rise to a further decrease in immobilization capacity as a result of the reduction in textural properties after the incorporation of nanosized iron oxide ferrites. Thus, at a pH 10, the amounts of lysozyme adsorbed are in the ranges 350−500 mg g^{-1} and 300−400 mg g^{-1} for the F20S (Figure 7b) and F32S (Figure 7c) series, respectively. These results show that in spite of the incorporation of the ferrite nanoparticles, the amount of lysozyme adsorbed still remains high, thereby confirming the capacity of magnetic nanocomposites to immobilize enzymes.

The above results show the importance of the pH of the solution for determining the amount of enzyme immobilized. The effect of the pH can be assessed by taking into account two factors: (a) the electrostatic interactions between the silica surface and the enzyme and (b) the lateral electrostatic repulsions between the adsorbed biomolecules. On the basis of the values for the isoelectric points (pI) of the free (nonadsorbed) lysozyme (pI 11) and silica (pI ≈ 2−3),[24] it can be postulated that for the pH range between the isoelectric points, an electrostatic attraction occurs between the positively charged biomolecules and the silica surface, as the latter contains a high surface density of negative charges associated with silanol

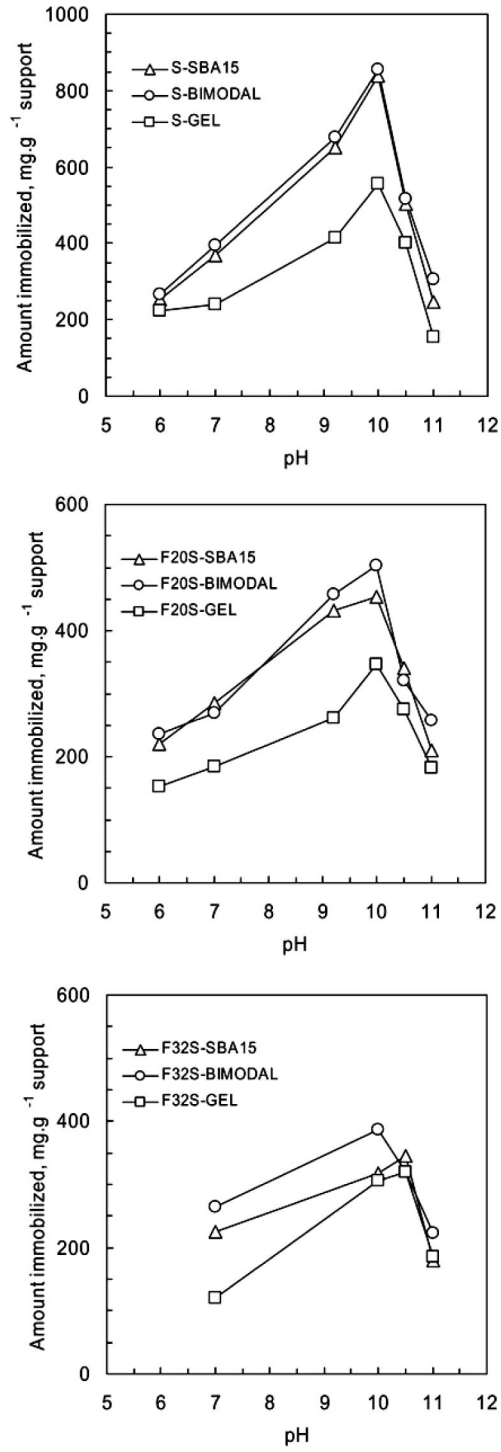

Figure 7. Modification of the amount of lysozyme immobilized with pH of solution for (a) the silica samples and magnetic composites with (b) 20 and (c) 32 wt % ferrite.

(24) (a) Su, T. J.; Green, R. J.; Wang, Y.; Murphy, E. F.; Lu, J. R.; Ivkov, R.; Satija, S. K. *Langmuir* **2000**, *16*, 4999. (b) Su, T. J.; Lu, J. R.; Thomas, R. K.; Cui, Z. F.; Penfold, J. *J. Colloid Interface Sci.* **1998**, *203*, 419. (c) Humphrey, H. P. Y.; Wright, P. A. *J. Mater. Chem* **2005**, *15*, 3690.

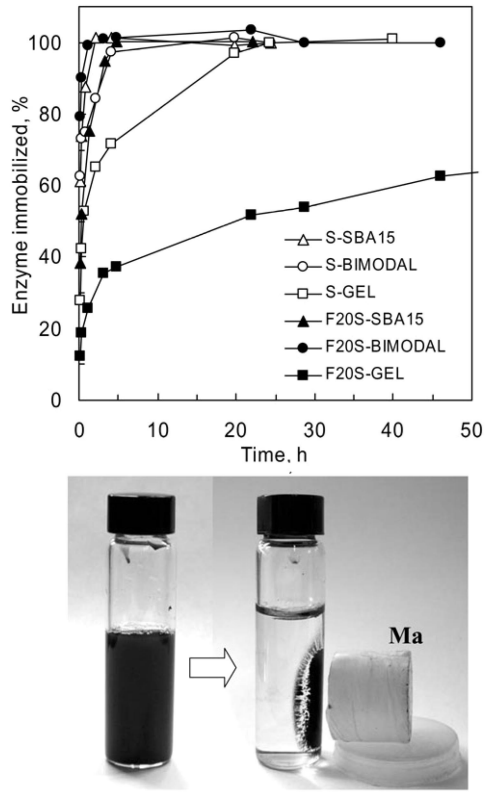

Figure 8. (a) Variation of the percentage of lysozyme adsorbed at pH 10.5 with the time. (b) Example of magnetic separation using a F202S-SBA15 composite loaded with lysozyme (pH 10).

groups. At the same time, lateral repulsions occur between the positively charged enzyme molecules, which restrict their adsorption. This effect diminishes as the pH of the solution increases because of a reduction in the net charge density of the biomolecules, which explains the increase in the amount of lysozyme adsorbed as the pH increases. Several authors have indicated that maximum enzyme adsorption occurs when the net charge of the adsorbed enzyme is zero (isoelectric point).[15b,24] This is because in these conditions, the absence of lateral repulsions between the adsorbed biomolecules will ensure that they are densely packed. The results shown in Figure 7 clearly indicate that the amount adsorbed attains a maximum at a pH 10 and not at pH 11, as one might have expected from the pI of the free (nonadsorbed) lysozyme. Vinu et al. observed a similar deviation in the maximum uptakes of lysozyme on the SBA-15 and MCM-41 substrates.[15]b This behavior can be attributed to the fact that the zero net charge point of the enzyme shifts from pH 11 for the free lysozyme to lower pH values for the adsorbed enzyme (sorbent−enzyme complex), as Haynes and Norde have already explained.[25]

Figure 8a shows the variation with time in the amount of lysozyme immobilized by silica and the magnetic nanocomposites (20 wt % ferrite) at a pH 10.5. A comparison of the immobilization trends for the silica samples and the composites shows that the insertion of magnetic nanoparticles causes a reduction in the immobilization rate only in the case of the F20S-GEL based composites. A comparison of the adsorption kinetics of the silica samples and other composites shows similar trends at all pH values. These results indicate that the insertion of magnetic nanoparticles into the pores of S-SBA15 or the S-BIMODAL silica matrices does not entail any significant restriction to the diffusion of lysozyme molecules. Furthermore, an important advantage of employing magnetic composites to immobilize biomolecules is that they can be easily recovered from the reaction media by means of an external magnetic field (see inset in Figure 8b).

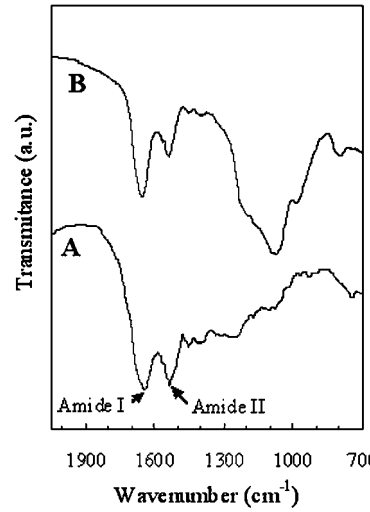

Figure 9. FTIR spectra of (A) free lysozyme and (B) F20S-SBA15 composite loaded with lysozyme. The band at 900−1300 cm^{-1} in trace B is associated with the Si−O−Si groups present in the silica composite.

To analyze the structural stability of the immobilized lysozyme, FTIR spectra of the free lysozyme and magnetic composite (F20S-SBA15) loaded with lysozyme were recorded (Figure 9). The spectrum of the free lysozyme exhibits two characteristic peaks at ∼1650 and at ∼1530 cm^{-1} denoted as amide bands I and II, which are due to the C═O stretching mode and the bending and stretching mode of the N−H and C−N vibrations, respectively.[15b,16a,b] These bands also appear in the spectrum corresponding to the lysozyme adsorbed by the magnetic composite, which shows that the secondary structure of the enzyme remains intact after immobilization.

Conclusions

In summary, we present a methodology for preparing iron oxide/silica nanocomposites characterized by a large BET surface area, a high pore volume, at least one pore size population greater than ∼10 nm, and a superparamagnetic functionality provided by iron oxide nanosized spinel ferrites. We found that magnetic nanocomposites with a monomodal and ordered mesostructured porosity, a high BET surface area and high pore volume values, display good magnetic properties as a result of a better distribution, and lower size dispersion of the magnetic component. Moreover, the magnetic nanocomposites from the bimodal silica and commercial silica gel show

(25) Haynes, C. A.; Norde, W. *Colloids Surf., B* **1994**, *2*, 517.

significant magnetic dipolar interactions. The effectiveness of these magnetic composites for the immobilization and magnetic separation of biomolecules has been clearly demonstrated in the case of lysozyme. These composites are able to immobilize large amounts of enzyme. For both the silica samples and the magnetic composites, lysozyme uptake varies significantly with the pH, exhibiting a maximum at a pH 10. The insertion of magnetic nanoparticles into the S-SBA15 and S-BIMODAL samples has no significant effect on the adsorption rate of the enzyme molecules. The FTIR spectrum obtained for the composite loaded with lysozyme shows that the structure of this biomolecule is preserved after its immobilization.

Acknowledgment. The financial support for this research provided by the MCyT (MAT2008-00407 and MAT2008-03224/NAN) is gratefully acknowledged.

CM8005937